Data-driven and physics-based interval modelling of power spectral density functions from limited data

Marco Behrendt[a,*], Chao Dang[a], Michael Beer[a,b,c]

[a]*Institute for Risk and Reliability, Leibniz Universität Hannover, Callinstraße 34, 30167 Hannover, Germany*
[b]*Institute for Risk and Uncertainty, University of Liverpool, Peach Street, Liverpool L69 7ZF, United Kingdom*
[c]*International Joint Research Center for Resilient Infrastructure & International Joint Research Center for Engineering Reliability and Stochastic Mechanics, Tongji University, 1239 Siping Road, Shanghai 200092, China*

Abstract

In stochastic dynamics, ensuring the structural reliability of buildings and structures is of paramount importance, especially when subjected to environmental loads such as wind or earthquakes. To adequately address these loads and the uncertainties associated with them, it is often necessary to utilise advanced load models, frequently expressed using a power spectral density (PSD) function. The construction of these load models becomes challenging when only limited data is available and meaningful statistics cannot be reliably derived. To address this issue, safety bounds are commonly used in load models to account for uncertainties. Many PSD functions, such as the Clough-Penzien model, are described by parameters with a physical background and can therefore reflect the real case. The aim of this work is to expand these physical parameters in order to account for uncertainties. For this purpose, bootstrapping is used to derive more reliable statistics. By introducing a scaling parameter that allows for flexibility, bounds of the data set can be derived. Consequently, suitable PSD models are fitted to the derived bounds. The PSD function is thus represented by intervals for its physical properties instead of relying on discrete values. When applying such a bounded load model to a structure, advanced interval propagation schemes can be utilised to bound the failure probability.

Keywords: Power spectral density function, Random vibrations, Stochastic processes, Stochastic dynamics, Uncertainty quantification.

1. Introduction

The ever-increasing demands for safer and more robust structures have led researchers and engineers to explore new avenues in the assessment of structural reliability. Traditional design approaches that rely solely on deterministic methods can fail to recognise the profound impact of uncertainties that occur in real-world scenarios. Stochastic dynamics [1, 2, 3, 4] and structural reliability [5, 6] offer a useful approach to model and integrate loads and material properties probabilistically or imprecisely, allowing for a more comprehensive understanding of structural behaviour under random excitations, such as earthquakes or wind loads.

The power spectral density (PSD) function [7, 8] is a key tool in the study of stochastic dynamics and plays a crucial role in evaluating the response of structures subjected to random excitations. It provides a representation of a stochastic process in the frequency domain or for more realistic cases in the time-frequency domain [9, 10, 11], which result in so-called *evolutionary* PSD (EPSD) functions. It enables to understand the distribution of power across different frequencies. The PSD function provides a relationship between the time domain and the frequency domain and enables easier analysis of structures under stochastic loads. By applying the concept of the PSD function, engineers can transform the problem of evaluating the structural response to random loads into a simpler frequency domain problem. This transformation facilitates the identification of critical resonant frequencies and enables the design of structures with better resistance to vibrations caused by dynamic loads. Including the PSD function in structural reliability analysis allows for a more realistic representation of the loads. Real world dynamic loads, such as earthquakes, wind loads or ocean waves have random characteristics in terms of both amplitude and frequency content. The PSD function allows for capturing these statistical characteristics and take them into account in reliability assessment to ensure that structures are designed to withstand certain dynamic excitations. Despite its merits, working with the PSD function may present

*Corresponding author
Email address: behrendt@irz.uni-hannover.de (Marco Behrendt)

challenges, particularly when dealing with non-stationary processes or limited experimental data. Addressing these challenges requires innovative techniques in signal processing and statistical analysis, as well as advancements in data-driven approaches to estimate the PSD function accurately.

In cases where the availability of data is limited, it is important construct robust models for the PSD function, thus an adaptable approach becomes imperative. Three distinct avenues can be identified for addressing this challenge: (i) a strictly data-driven methodology without explicitly incorporating physical principles, (ii) a purely physics-based approach, reliant solely on theoretical formulations without direct data influence and (iii) a synergistic approach that combines data-driven and physics-based aspects. In this research, the third approach is selected due to its potential to combine the strengths of data-driven techniques with the physical principles of PSD functions and corresponding stochastic processes. This strategy not only accommodates limited data scenarios, but also takes advantage of the improved performance that can be achieved by incorporating available physical knowledge into the modelling process. The aim is to provide a comprehensive framework that uses the advantages of both data and physics-based knowledge to construct reliable and accurate PSD models, thereby contributing to an understanding of the underlying system dynamics.

While stochastic dynamics and structural reliability offer a promising approach for designing new structures, several challenges arise when dealing with real-world data, especially in the context of estimating PSD functions and assessing structural reliability. Often, only limited experimental data or historical records are available, leading to uncertainties especially in estimating a reliable PSD function. The lack of data can affect the accuracy of PSD estimation and thus lead to incorrect reliability analysis. Measurement errors and uncertainties are a critical aspect as they can significantly affect the accuracy and reliability of experimental data used for analysis and design. These uncertainties arise from various sources, such as equipment limitations, sensors which may calibrated inaccurately, environmental conditions or simply due to the digitisation of data [12]. Understanding and quantifying these uncertainties is critical to perform reliable probabilistic analyses. Some general approaches in the field of uncertainty quantification have already been carried out.

These can be broadly divided into probabilistic approaches [13], interval approaches [14] or imprecise probabilities [15]. More specifically, approaches for problems under limited data can be tackled by [16, 17] or many more.

The main focus of many works is to establish reliable bounds for a given set of data or parameters. Some approaches in this area have already been addressed. The bounding of the failure probability based on different interval parameters of PSD models has been carried out in [18]. A large set of accelerograms was utilised in [19] to determine different representations of PSD function. In [20], a limited number of PSD functions are used to determine an upper and lower bound using radial basis function networks. However, it is crucial to question the reliability of such bounds, especially when dealing with limited data. This paper addresses the problem of uncertain bounds. It aims to increase the credibility of limited data approaches by addressing the reliability of the resulting bounds. On many occasions, the available data is limited, thereby requiring an assessment of the accuracy of the bounds. This approach attempts to address these concerns and introduce flexibility in the definition of these bounds.

The goal of this work is to determine bounds for the physical parameters of an analytical PSD function, such as the Kanai-Tajimi PSD [21, 22] model or the Clough-Penzien PSD model [23]. This is carried out by a data-driven bootstrapping approach for the quantification of uncertainties. The key aspect of this approach is the introduction of a scaling parameter that allows the setting of bounds based on expert knowledge and statistical properties of the data set. This allows for the selection of more conservative or less conservative bounds, providing some flexibility in the modelling of the bounds. To illustrate the practicality of this method, consider the following scenario: Data have been collected from only one monitoring station in an area where the construction of new buildings is planned. By using the existing data from the measuring station, it is possible to define intervals for the physical parameters. Consequently, best-case and worst-case scenarios can be created for this location, enabling informed decision-making and better planning and including site-specific information, such as the soil properties. Further, by fitting physical based models to the data, uncertainties due to PSD estimators can be reduced.

This work is organised as follows: In Section 2 some preliminaries necessary for this work will be introduced. The proposed procedure for developing a load model accounting for uncertainties is illustrated in Section 3 for the stationary case and for the non-stationary case, where both, the separable and non-separable EPSD will be utilised. Real data records are utilised in Section 4 to derive the bounds and to show the methods feasibility and flexibility for real world cases. The work concludes in Section 5 with some final remarks.

2. Preliminaries

In this section, a brief overview of the fundamental concepts essential for the context of this work is provided.

2.1. Stochastic processes

The Wiener-Khintchine theorem (e.g. [3, 11, 7]) is an important relation in the field of stochastic processes. It establishes a fundamental link between the power spectral density (PSD) function $S_X(\omega)$ of a signal and its autocorrelation function $R_X(\tau)$ with τ as time lag. The theorem states that the Fourier transform of the autocorrelation function of a stochastic process is equal to the PSD function of that signal

$$S_X(\omega) = \frac{1}{2\pi} \int_{-\infty}^{\infty} R_X(\tau) e^{-i\omega\tau} d\tau, \tag{1}$$

while the inverse Fourier transform yields the vice versa result

$$R_X(\tau) = \int_{-\infty}^{\infty} S_X(\omega) e^{i\omega\tau} d\omega. \tag{2}$$

The theorem is particularly useful when dealing with random or stochastic signals where conventional time-domain analysis does not provide sufficient insight. It allows to analyse the frequency content of signals and to understand how their power is distributed over different frequencies. By transforming the signal into the frequency domain, dominant frequency components can be identified and the spectral properties of the signal can be investigated. While the Wiener-Khintchine theorem establishes a theoretical relationship between the PSD and autocorrelation function, PSD estimators play a crucial role in practical applications.

The theorem assumes that the signal is wide-sense stationary and has an infinite length in time, which is not fulfilled in real world applications. Further, the theorem holds for stationary processes only. Earthquakes, for instance, have a strongly transient character, so that other techniques have to be resorted to.

2.1.1. PSD and EPSD estimation

In this section, PSD estimation for both stationary and non-stationary PSDs, often referred to as EPSDs, is briefly described. The stationary PSD estimation can be computed using the periodogram, for instance, which is based on the discrete Fourier transform [8]. The periodogram is given to be

$$\hat{S}_X(\omega_k) = \frac{1}{N_t}\left|\sum_{t=0}^{N_t-1} x_t e^{-\frac{i2\pi}{N_t}kt}\right|^2, \tag{3}$$

where $\hat{S}_X$ denotes the PSD estimate, N_t is the number of points in time, x_t is the value of the t-th time instant and k is the integer frequency for $\omega_k = \frac{2\pi k}{T}$, where T is the total length of the time record. Other methods to estimate the stationary PSD are, for instance, Bartlett's method [24, 25] or Welch's method [26]. Since these methods work by segmenting and averaging the time signal, they usually provide smoother estimates than the periodogram.

As stochastic processes often have an inherent non-stationary character (e.g. earthquakes have a short term transient behaviour), the estimation of the EPSD will result in a more reliable and more realistic representation. The EPSD is a transformation from time domain to time-frequency domain and accounts for temporal changes in the frequency content of the process. Various methods for estimating the EPSD are available, including but not limited to the short-time Fourier transform, the Priestley method [9], and Wavelet-based methods [27, 28]. However, in this work, the recently developed multi-taper S-transform (MTST) [29, 30] will be utilised as it yields results in a good resolution and is able to reduce the estimation variance. The MTST estimation is given to be

$$\hat{S}_X(\omega, t) = \frac{1}{M}\sum_{m=0}^{M-1} s_m^*(\omega, t) s_m^T(\omega, t), \tag{4}$$

where the S-transform $s_m(\omega,t)$ and its complex conjugate $s_m(\omega,t)^*$ of a non-stationary stochastic process $U(t)$ is

$$s_m(\omega,t) = \sum_{k=-\infty}^{\infty} \Psi_m(\omega, k\Delta t - t) U(k\Delta t) e^{-i2\pi\omega k\Delta t} \Delta t. \tag{5}$$

In this equation, the orthogonal time-frequency Hermite windows $\Psi_0(\omega,t)$ for the zeroth-order is

$$\Psi_0(\omega,t) = \pi^{-0.25}\sqrt{w(\omega)} e^{-0.5w^2(\omega)t^2}, \tag{6}$$

while $\Psi_1(\omega,t)$ for the first-order yields

$$\Psi_1(\omega,t) = \sqrt{2}\pi^{-0.25} w^{1.5}(\omega) t e^{-0.5w^2(\omega)t^2}, \tag{7}$$

and any higher order $\Psi_m(\omega,t)$ for $m > 1$ is

$$\Psi_m(\omega,t) = \sqrt{\frac{2}{m}} w(\omega) t \Psi_{m-1}(\omega,t) - \sqrt{\frac{m-1}{m}} \Psi_{m-2}(\omega,t). \tag{8}$$

2.1.2. Stochastic process generation

For the generation of stochastic processes used in simulations, the spectral representation method (SRM) [31] can be utilised. The method requires an analytical or estimated expression of a PSD function $S(\omega)$ and yields a stochastic process X_t in time domain, carrying the spectral characteristics of the underlying PSD function. SRM reads as follows

$$X_t = \sqrt{2} \sum_{n=0}^{N_\omega - 1} \left(2S(\omega_n)\Delta\omega\right)^{1/2} \cos(\omega_n t + \varphi_n), \tag{9}$$

where $n = 0, 1, \dots, N_\omega - 1$, N_ω as the number of frequency components, $\Delta\omega$ as frequency discretisation, $\omega_n = n\Delta\omega$ as frequency coordinates, the φ_n's describe independent random phase angles in the range $[0, 2\pi]$ and t is the time vector.

Equivalently, non-stationary stochastic processes can be generated based on an underlying EPSD function $S(\omega,t)$ by an extension of SRM to its non-stationary case [32]. In this case, the stationary PSD function $S(\omega_n)$ is replaced by its non-stationary equivalent $S(\omega,t)$

$$X_t = \sqrt{2} \sum_{n=0}^{N_\omega - 1} \left(2S(\omega_n, t)\Delta\omega\right)^{1/2} \cos(\omega_n t + \varphi_n). \tag{10}$$

2.2. Bootstrap sampling

Bootstrap sampling is a resampling technique widely employed in statistics and machine learning to address the challenge of estimating the sampling distribution of a statistic or making inferences about a population based on a single sample, see for instance [33]. It has since become a fundamental tool in data analysis. The basic idea behind bootstrap sampling involves generating numerous "pseudo-samples" from the original samples by randomly selecting data points from it with replacement. Each pseudo-sample may contain duplicate observations and omit others, effectively mimicking the randomness of drawing samples from the population. By calculating the statistic of interest (e.g., mean, median, confidence interval) for each of these pseudo-samples and examining the distribution of these bootstrap statistics, analysts can make robust inferences about the population or assess the variability of their estimates. Bootstrap sampling is particularly advantageous because it does not rely heavily on assumptions about the population's distribution and can be applied to various statistical problems, offering a versatile tool for data analysis.

3. Method development

To enhance the statistical robustness of the limited PSD functions, a bootstrapping approach applied to individual frequencies was employed. This method involved generating pseudo-samples, often referred to as bootstrap samples, through random sampling with replacement. These pseudo-samples simulate multiple instances of the original data, allowing for a more comprehensive assessment of the variability in spectral estimates. By applying bootstrapping independently to each frequency component in the PSD functions, more reliable estimates of statistical quantitites, such as mean and standard deviation, for instance, can be obtained. This resampling technique offers a powerful means of assessing the variability of spectral estimates, particularly in regions where the only limited data is available. The resulting bootstrapped statistics, based on these pseudo-samples, not only provide a comprehensive understanding of the central tendencies and uncertainties associated with each frequency but also enable the computation of more reliable maximum and minimum spectra. This method effectively mitigates problems associated with limited data sets, which contributes to the overall robustness of the spectral analysis, enhancing the credibility of the findings.

The bootstrap sampled minimum spectrum $S^{BS}_{\min}$ and maximum spectrum $S^{BS}_{\max}$ are

$$S^{BS}_{\min}(\omega_n) = \min(S^{BS}_i(\omega_n)) \; \forall \; i \in N_{BS} \tag{11}$$

and

$$S^{BS}_{\max}(\omega_n) = \max(S^{BS}_i(\omega_n)) \; \forall \; i \in N_{BS}, \tag{12}$$

with N_{BS} as number of bootstrap samples. Similarly, the standard deviation of the bootstrap samples will be determined from all bootstrap samples

$$\sigma^{BS}_{\min}(\omega_n) = \sqrt{\frac{1}{N_{BS}-1} \sum_{i=1}^{N_{BS}} \left(S^{BS}_i(\omega_n) - S^{BS}_{\min}(\omega_n)\right)^2} \tag{13}$$

and

$$\sigma^{BS}_{\max}(\omega_n) = \sqrt{\frac{1}{N_{BS}-1} \sum_{i=1}^{N_{BS}} \left(S^{BS}_i(\omega_n) - S^{BS}_{\max}(\omega_n)\right)^2}. \tag{14}$$

By introducing a scaling factor λ, the *augmented* bounds result in

$$\underline{S}^{aug}(\omega_n) = S^{BS}_{\min}(\omega_n) - \lambda \sigma^{BS}_{\min}(\omega_n) \tag{15}$$

and

$$\overline{S}^{aug}(\omega_n) = S^{BS}_{\max}(\omega_n) + \lambda \sigma^{BS}_{\max}(\omega_n). \tag{16}$$

The equations presented here demonstrate the procedure for PSD functions. When using EPSD functions, the same approach can be used, whereby the respective functions are extended by the time parameter. The scaling factor $\lambda \in \mathbb{R}$ has to be determined by the analyst and shall be selected properly, in the optimal scenario with the integration of expert knowledge. Some suggestions on how to choose λ are given in Section 3.1. Handling the bounds in such a way offers several advantages: flexibility, case-dependent adjustment, iterative approach. If the scaling factor λ is chosen too large, negative values in the augmented bounds can occur. Since spectral densities are non-negative by nature, those can simply be set to zero.

Separate upper and lower bound optimisations are performed to fit a PSD model S^{model} and its corresponding set of parameters $\boldsymbol{\theta}$ to the augmented bounds determined by bootstrapping. The objective function for the optimisation is specified by the least squares solution between the augmented bounds and the chosen model. The optimisation for the lower bounds in the stationary case reads

$$f\left(\underline{\boldsymbol{\theta}}\right) = \min_{\underline{\boldsymbol{\theta}}} \quad \sum_{n=1}^{N_\omega} \left(\underline{S}^{aug}(\omega_n) - S^{model}\left(\omega_n, \underline{\boldsymbol{\theta}}\right)\right)^2, \tag{17}$$

while the upper bound can be optimised via

$$f\left(\overline{\boldsymbol{\theta}}\right) = \min_{\overline{\boldsymbol{\theta}}} \quad \sum_{n=1}^{N_\omega} \left(\overline{S}^{aug}(\omega_n) - S^{model}\left(\omega_n, \overline{\boldsymbol{\theta}}\right)\right)^2. \tag{18}$$

In case a more realistic EPSDs is utilised, the optimisation for the lower bound yields

$$f\left(\underline{\boldsymbol{\theta}}\right) = \min_{\underline{\boldsymbol{\theta}}} \quad \sum_{n=1}^{N_\omega} \sum_{m=1}^{N_t} \left(\underline{S}^{aug}(\omega_n, t_m) - S^{model}\left(\omega_n, t_m, \underline{\boldsymbol{\theta}}\right)\right)^2, \tag{19}$$

whereas the upper bound can be optimised by

$$f\left(\overline{\boldsymbol{\theta}}\right) = \min_{\overline{\boldsymbol{\theta}}} \quad \sum_{n=1}^{N_\omega} \sum_{m=1}^{N_t} \left(\overline{S}^{aug}(\omega_n, t_m) - S^{model}\left(\omega_n, t_m, \overline{\boldsymbol{\theta}}\right)\right)^2. \tag{20}$$

In these equations $\underline{\boldsymbol{\theta}}$ and $\overline{\boldsymbol{\theta}}$ represents the particular set of parameters needed for the specific model. Once the model and the corresponding parameters are fitted to the augmented bounds, interval parameters result which can be used to sample individual PSD functions in subsequent simulations. Thus, the best-case or worst-case scenario can be determined within the framework of a reliability analysis.

3.1. Selection of the scaling parameter λ

The scaling parameter plays a pivotal role in enhancing the adaptability of models for bounding purposes. However, it is crucial to exercise caution when selecting its value, as arbitrary choices may lead to undesirable consequences. An excessively high scaling parameter can result in unreasonably large bounds, thereby increasing the failure probability beyond acceptable limits, which contradicts the intended outcome. Conversely, an inadequately small parameter fails to adequately quantify or incorporate uncertainties into the model. To address this challenge, this study explores a potential solution to establish an appropriate scaling parameter by examining the characteristics of generated stochastic processes. This approach aims to provide deeper insights into the scaling parameter's properties prior to conducting simulations.

To address the challenge of determining a suitable scaling parameter, the study proposes an approach that involves a comprehensive examination of the stochastic processes generated within the model. Through a comprehensive examination of these processes, a deeper understanding of the scaling parameter's behaviour and characteristics is sought. This understanding is crucial in ensuring that the chosen scaling parameter aligns with the desired level of uncertainty representation. Furthermore, the possibility of comparing the scaling parameter with established seismic metrics like peak ground acceleration (PGA) is investigated. This comparison allows to leverage existing knowledge of the statistical properties of the stochastic processes from which the model is derived and to assess the scaling parameter's appropriateness in the context of specific ground motions occurring within the study area. Such an integrative approach enhances the ability to make informed decisions regarding the scaling parameter's value, ultimately leading to more robust and accurate simulations.

3.2. Artificial examples

The procedure is illustrated covering different cases with artificially generated data, in particular for a stationary PSD model, a non-separable EPSD model and a separable EPSD model. Each of the three limited data sets was generated using an analytical PSD/EPSD model to reflect the underlying physics. From this, artificial stochastic processes were generated using SRM (Eq. 9 or Eq. 10). These were considered as "recorded data", at least for the artificial examples, and transformed into the frequency domain (Eq. 3) or time-frequency domain (Eq. 4) via the corresponding estimators. Based on these resulting ensemble of

PSD/EPSD functions, the previously described approach will be illustrated. Further, these examples serve for comparison and validation if the feasible parameters were found. In all cases, a number of 10,000 bootstrap samples were generated based on the limited data set to obtain reliable statistics.

3.2.1. Stationary power spectral density function

In the stationary case two typical models used are the Kanai-Tajimi PSD model [21, 22] and the Clough-Penzien PSD model [23]. The Kanai-Tajimi PSD model reads as

$$S^{KT}\left(\omega, \boldsymbol{\theta}^{KT}\right) = S_0 \cdot \frac{\omega_g^4 + 4\zeta_g^2\omega_g^2\omega^2}{\left(\omega_g^2 - \omega^2\right)^2 + 4\zeta_g^2\omega_g^2\omega^2}, \tag{21}$$

with $\boldsymbol{\theta}^{KT} = [S_0, \omega_g, \zeta_g]$. The Kanai-Tajimi PSD model passes a white noise process through a linear soil filter determined by the natural frequency ω_g and damping ζ_g, respectively, while S_0 determines the spectral intensity, see for instance [34]. A drawback of the Kanai-Tajimi PSD model is that velocity and displacement are not defined for frequencies which tend to zero, i.e. $\omega \to 0$. To overcome this issue, the Clough-Penzien model was defined by expressing the Kanai-Tajimi PSD function with an additional filter determined by frequency ω_f and damping ζ_f

$$S^{CP}\left(\omega, \boldsymbol{\theta}^{CP}\right) = S_0 \cdot \frac{\omega^4}{\left(\omega_f^2 - \omega^2\right)^2 + 4\zeta_f^2\omega_f^2\omega^2} \cdot \frac{\omega_g^4 + 4\zeta_g^2\omega_g^2\omega^2}{\left(\omega_g^2 - \omega^2\right)^2 + 4\zeta_g^2\omega_g^2\omega^2}, \tag{22}$$

with $\boldsymbol{\theta}^{CP} = [S_0, \omega_g, \zeta_g, \omega_f, \zeta_f]$, see [23, 34] for instance.

In this example, the Clough-Penzien PSD model will be utilised due to its realistic behaviour. Three stochastic processes are generated based on the Clough-Penzien PSD model utilising the parameters $S_0 = 1$, $\omega_f = 0.5\pi$, $\zeta_f = 0.6$, $\omega_g = 5\pi$ and $\zeta_g = 0.6$, which are adopted from [35], while the upper cut-off frequency is set to $\omega_u = 80$ rad/s. The resulting ensemble of PSDs is depicted in Fig. 1.

The augmented bounds are derived using Eqs. 15 and 16 with scaling parameter $\lambda = 1.5$. The specific optimisation problems to be solved for lower and upper bound are

$$f\left(\underline{\boldsymbol{\theta}}^{CP}\right) = \min_{\underline{\boldsymbol{\theta}}^{CP}} \quad \sum_{n=1}^{N_\omega} \left(\underline{S}^{aug}\left(\omega_n\right) - S^{CP}\left(\omega_n, \underline{\boldsymbol{\theta}}^{CP}\right)\right)^2 \tag{23}$$

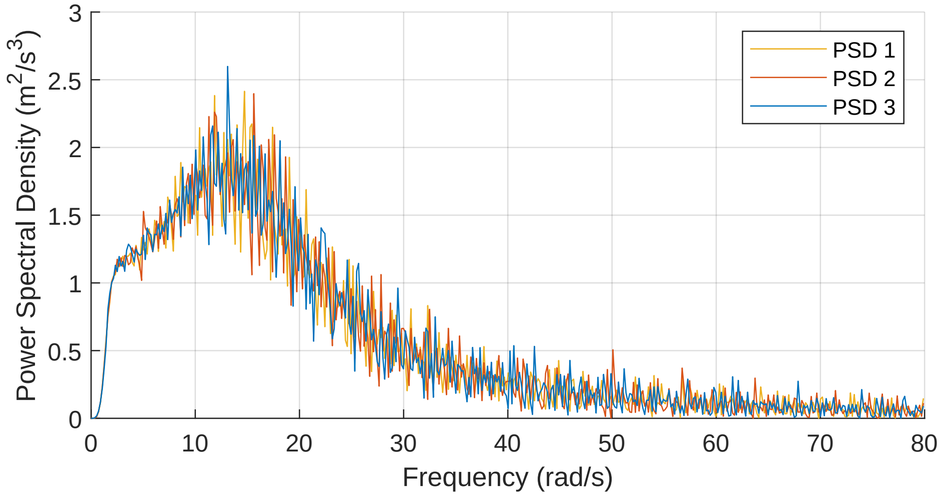

Figure 1: Ensemble of the Clough-Penzien PSDs.

Table 1: Identified parameters for the Clough-Penzien PSD model.

	S_0	ω_f	ζ_f	ω_g	ζ_g
$S^{CP}(\omega, \underline{\boldsymbol{\theta}}^{CP})$	0.7517	1.7680	0.4809	13.9162	0.5666
$S^{CP}(\omega, \overline{\boldsymbol{\theta}}^{CP})$	1.2407	1.3413	0.7552	16.7373	0.6270

and

$$f\left(\overline{\boldsymbol{\theta}}^{CP}\right) = \min_{\overline{\boldsymbol{\theta}}^{CP}} \sum_{n=1}^{N_\omega} \left(\overline{S}^{aug}\left(\omega_n\right) - S^{CP}\left(\omega_n, \overline{\boldsymbol{\theta}}^{CP}\right)\right)^2. \tag{24}$$

An example of this procedure is depicted in Fig. 2, while the fitted parameters are given in Table 1. The corresponding objective function values are $f\left(\underline{\boldsymbol{\theta}}^{CP}\right) = 7.6833$ and $f\left(\overline{\boldsymbol{\theta}}^{CP}\right) = 9.4891$. The relatively high values can be explained by the highly variant PSD functions in Fig. 2. The resulting bounds deliver very smooth results, while the derived augmented bounds are relatively variant. The general shape is captured well by the optimised bounds.

3.2.2. Non-separable evolutionary power spectral density function

An example for a non-separable EPSD function is given in [36], for instance, which is used in a generalised form in this work

$$S^{non-sep}\left(\omega, t, \boldsymbol{\theta}^{non-sep}\right) = S_0 \left(\frac{\omega}{\omega_g}\right)^2 e^{ct} t^2 \exp\left(-\left(\frac{\omega}{\omega_g}\right)^2 t\right). \tag{25}$$

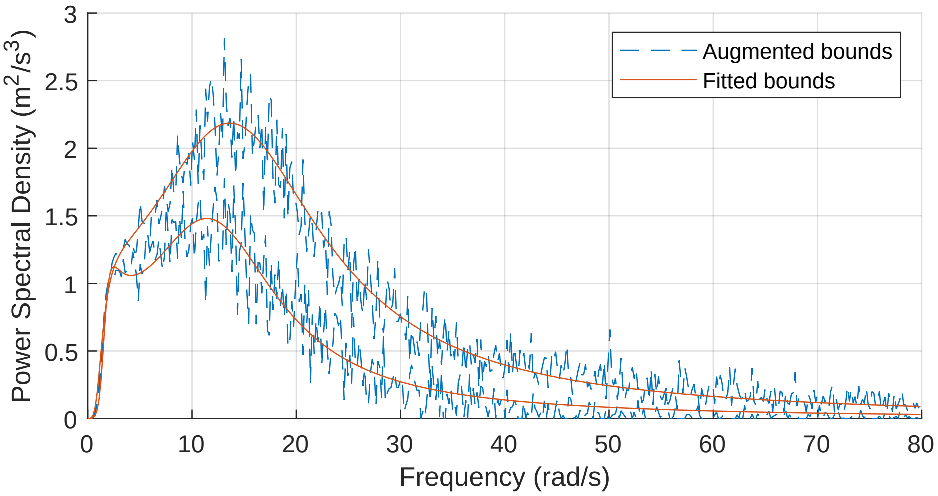

Figure 2: Example of the Clough-Penzien model fitted to the augmented bounds with scaling parameter $\lambda = 1.5$.

This model can be described by the parameters $\boldsymbol{\theta}^{non-sep} = [S_0, c, \omega_g]$. For generating the ensemble of EPSDs, the parameters $S_0 = 1$, $c = -0.15$ and $\omega_g = 5\pi$ are utilised.

The specific optimisation problems to be solved for lower and upper bound with a scaling parameter of $\lambda = 2$ are

$$f\left(\underline{\boldsymbol{\theta}}^{non-sep}\right) = \min_{\underline{\boldsymbol{\theta}}^{non-sep}} \sum_{n=1}^{N_\omega} \sum_{m=1}^{N_t} \left(\underline{S}^{aug}(\omega_n, t_m) - S^{non-sep}\left(\omega_n, t_m, \underline{\boldsymbol{\theta}}^{non-sep}\right)\right)^2 \tag{26}$$

and

$$f\left(\overline{\boldsymbol{\theta}}^{non-sep}\right) = \min_{\overline{\boldsymbol{\theta}}^{non-sep}} \sum_{n=1}^{N_\omega} \sum_{m=1}^{N_t} \left(\overline{S}^{aug}(\omega_n, t_m) - S^{non-sep}\left(\omega_n, t_m, \overline{\boldsymbol{\theta}}^{non-sep}\right)\right)^2. \tag{27}$$

An example of this procedure is depicted in Fig. 3, while the corresponding optimised parameters are given in Table 2. Although it may appear that the optimised bounds closely resemble the augmented bounds, this is challenged by the notably high objective function values of $f\left(\underline{\boldsymbol{\theta}}^{non-sep}\right) = 200.8499$ and $f\left(\overline{\boldsymbol{\theta}}^{non-sep}\right) = 4406.5$. Despite these values, these bounds can still be considered for further analysis. The optimised bounds rely on the shape of the estimated EPSDs, which can exhibit a strong non-smooth behaviour, resulting in high objective values. However, the objective is to obtain approximate EPSD bounds that can be effectively utilised in simulations, thus those bounds are reasonable.

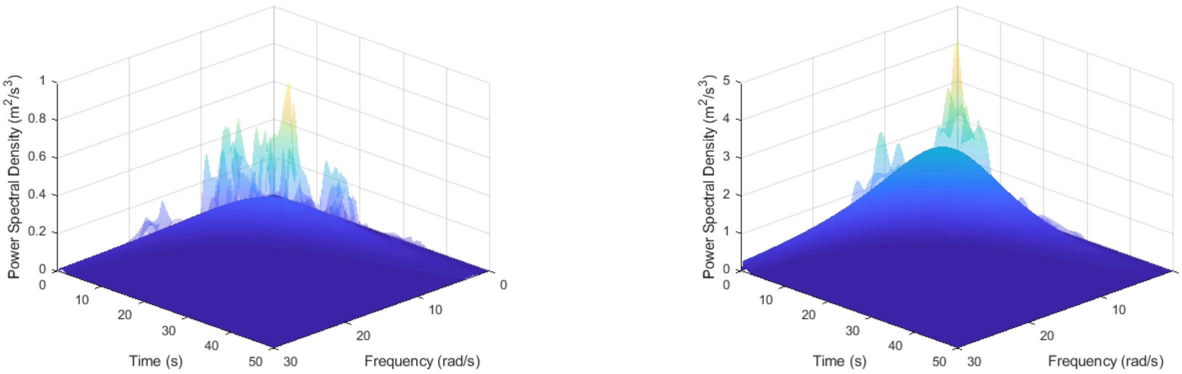

Figure 3: Comparison of augmented bounds and derived lower bound (left) and upper bound (right) for the non-separable EPSD model. The transparent representation shows the augmented bounds, the non-transparent ones are the fitted EPSDs. For both a scaling parameter of $\lambda = 2$ was utilised.

Table 2: Identified parameters for the non-separable EPSD model.

	S_0	c	ω_g
$S^{non-sep}\left(\omega, t, \underline{\boldsymbol{\theta}}^{non-sep}\right)$	0.1086	-0.1106	18.1903
$S^{non-sep}\left(\omega, t, \overline{\boldsymbol{\theta}}^{non-sep}\right)$	2.1590	-0.1508	15.6480

3.2.3. Separable evolutionary power spectral density function

A separable EPSD consists of a stationary PSD model, such as the Clough-Penzien model, and a time-modulating function, which will be multiplied with each other. The resulting separable EPSD function yields

$$S^{sep}(\omega, t) = S^{stationary}(\omega) g(t)^2. \tag{28}$$

The separable EPSD may offer more flexibility as the number of parameters in this specific case is higher than in the previous example. Further, this model can be adapted to different data sets or scenarios by replacing either the stationary PSD model $S^{stationary}$ or the time-modulating function $g(t)$. In the following example, the Clough-Penzien PSD described above (Section 3.2.1) will be utilised in combination with the time-modulating function

$$g_1(t) = k\left(e^{-at} - e^{-bt}\right), \tag{29}$$

with k as the scaling factor and a and b as shape parameters. The parameters utilised here are $k = 4$, $a = 0.25$ and $b = 0.5$. For reference, other time-modulating functions can be found Appendix A.

The resulting separable EPSD for this example yields

$$S^{sep}(\omega, t, \boldsymbol{\theta}^{sep}) = S^{CP}\left(\omega, \boldsymbol{\theta}^{CP}\right) g_1\left(t, \boldsymbol{\theta}^{t}\right)^2, \tag{30}$$

with $\boldsymbol{\theta}^{CP} = [S_0, \omega_g, \zeta_g, \omega_f, \zeta_f]$, $\boldsymbol{\theta}^t = [k, a, b]$ and thus $\boldsymbol{\theta}^{sep} = [\boldsymbol{\theta}^{CP}, \boldsymbol{\theta}^t]$. The derivation of the bounds is carried out with a scaling factor of $\lambda = 2$. The optimisation problems are thus

$$f\left(\underline{\boldsymbol{\theta}}^{sep}\right) = \min_{\underline{\boldsymbol{\theta}}^{sep}} \sum_{n=1}^{N_\omega} \sum_{m=1}^{N_t} \left(\underline{S}^{aug}(\omega_n, t_m) - S^{sep}\left(\omega_n, t_m, \underline{\boldsymbol{\theta}}^{sep}\right)\right)^2 \tag{31}$$

and

$$f\left(\overline{\boldsymbol{\theta}}^{sep}\right) = \min_{\overline{\boldsymbol{\theta}}^{sep}} \sum_{n=1}^{N_\omega} \sum_{m=1}^{N_t} \left(\overline{S}^{aug}(\omega_n, t_m) - S^{sep}\left(\omega_n, t_m, \overline{\boldsymbol{\theta}}^{sep}\right)\right)^2. \tag{32}$$

The resulting bounds are depicted in Fig. 4, while the corresponding parameters are given in Table 3. The objective function values are $f\left(\underline{\boldsymbol{\theta}}^{sep}\right) = 491.5593$ and $f\left(\overline{\boldsymbol{\theta}}^{sep}\right) = 7329.4$.

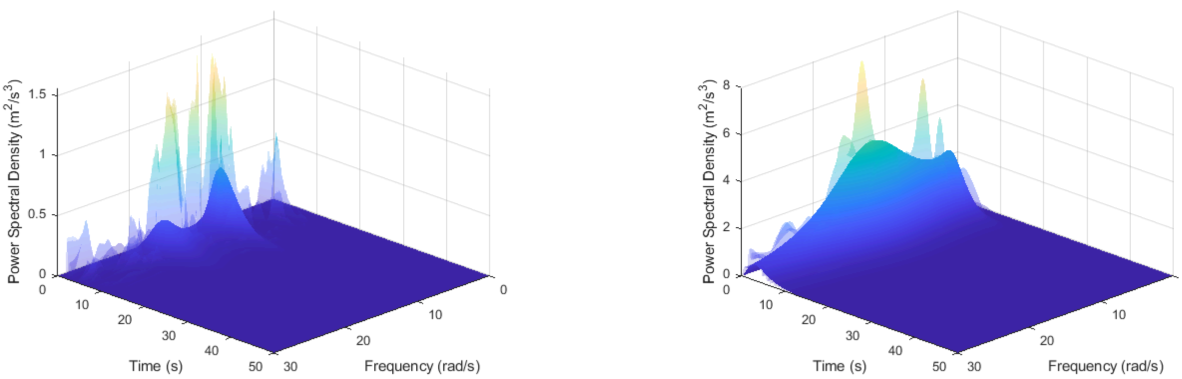

Figure 4: Comparison of augmented bounds and derived lower bound (left) and upper bound (right) for the separable EPSD model. The transparent representation shows the augmented bounds, the non-transparent ones are the fitted EPSDs. For both a scaling parameter of $\lambda = 2$ was utilised.

Here again, the derived bounds seem not to match well with the augmented bounds and again quite high objective values can be obtained. However, as before it can be argued that those bounds rely on the EPSD estimates, which are hardly ever smooth. Thus, although obtaining high objective values, the derived bounds can be used for further analysis.

Table 3: Identified parameters for the separable EPSD model.

	S_0	ω_f	ζ_f	ω_g	ζ_g	k	a	b
$S^{sep}(\omega, t, \underline{\boldsymbol{\theta}}^{sep})$	6.3859	9.5180	0.0702	17.7419	0.1057	10.8965	0.2593	0.2574
$S^{sep}\left(\omega, t, \overline{\boldsymbol{\theta}}^{sep}\right)$	7.7352	2.1889	0.4689	15.7403	0.4450	33.0126	0.3176	0.3299

3.3. Discussion on derived bounds

It is important to note that the parameters identified for the upper bound may not necessarily represent the uppermost values within their respective intervals. This observation is particularly pertinent in the context of specific models, such as the Clough-Penzien PSD model. In certain scenarios, increasing these parameters may unexpectedly lead to a reduction in the size of the PSD function itself. This counterintuitive behaviour can be attributed to the complex mathematical relationships inherent to the model, where higher parameter values may result in a more restricted or focused PSD function, rather than an expansion of its bounds.

An issue that arose during this investigation involved the generation of samples within predefined parameter bounds, some of which occasionally extended beyond these bounds, refer to Fig. 5. While this may initially seem counterintuitive, it's crucial to emphasise that the primary objective is to establish bounds for the underlying physical parameters, rather than strictly constraining the raw data itself. The focus lies in bounding the values associated with the physical characteristics of the system under examination.

In summary, the issue of samples occasionally exceeding parameter bounds aligns with the overarching goal of bounding the physical attributes of the system. Furthermore, it underscores the complexity of specific models, where adjusting parameter values may yield unexpected outcomes. Understanding and addressing these intricacies are essential for achieving accurate and meaningful results in the simulations.

In some cases the objective function values seem extremely high. In addition, the shapes of the augmented bounds compared to the ones derived through minimisation and optimising the parameters of the physical model often exhibits large differences due to the non-smoothness of the estimated PSD functions. Both issues can be explained very easily.

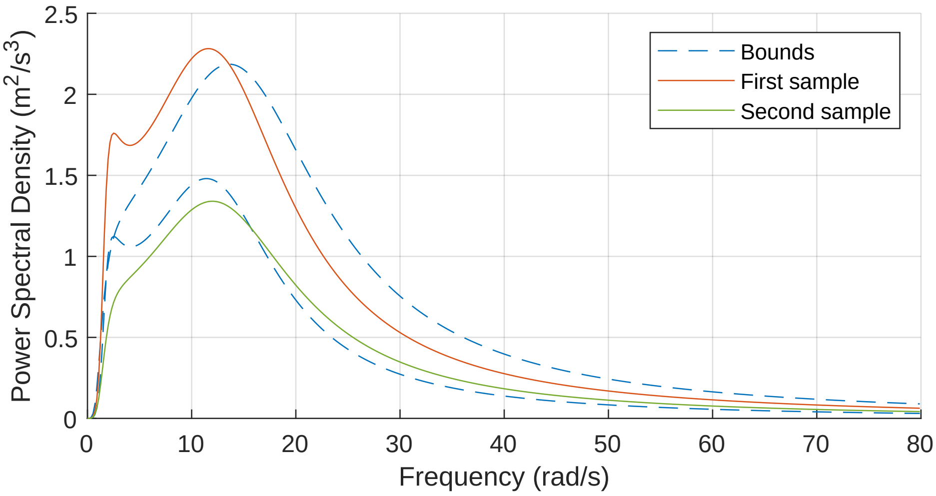

Figure 5: Example of generated samples which intersect the derived bounds.

The estimated PSDs and EPSDs have an immensely spiky behaviour, i.e. they often jump between high and low values between two frequency / time-frequency points. The fitted function, however, is smooth. By using the least squares as the objective function, this makes it impossible, nor desirable, to fit the function to the data perfectly. The function acts like a smoother of the data. Thus, it is logical that there are always high differences between the extreme value jumps. In the averaged sense, however, the fitted function adapts well. To overcome this issue, other PSD estimators may be used. For the stationary case Bartlett's method [24, 25] or Welch's method [26], as mentioned in Section 1, might be suitable, which usually result in a much smoother representation of the PSD and thus also most likely in a lower objective function.

However, the goal was to find, and specifically bound the respective parameters in order to capture the uncertainties induced by the limited data and the EPSD estimation process. For all cases, the PSD model and both EPSD models, bounded parameters can be derived. However, the parameters $\boldsymbol{\theta}$ utilised for generating the underlying ensembles are not always bounded by the derived interval parameter sets $\boldsymbol{\theta}^I$, however, this is also not a significant issue as the interaction of various parameters can influence these and thus deviate significantly from the original parameters. The objective was to identify parameters capable of characterising both the upper and lower bound of the spectral densities, and this objective has been successfully accomplished.

It's important to consider that in certain instances, it can be advantageous to pre-process the data appropriately. Too many spectral densities close to 0 in a large range, especially in the EPSD, can lead to undesired results and negatively influence the fitting. Large areas with spectral densities close to 0 also push the value of the objective function down very quickly, so that the optimisation algorithm quickly lies in a local minimum. Therefore, it is advisable to reduce the data set to the range where high spectral densities are obtained, i.e. the important range, and to cut off the parts where those densities are very close to zero (for example $S(\omega, t) \leq 10^{-5}$). This has the advantage that only the relevant spectral densities are considered in the fitting. Overall, this procedure has no disadvantages compared to fitting the entire range, since the determined parameters will be entered into an analytical function and the cut-off ranges can thus easily be included in the analytical function again.

4. Application to real data records

Within this section, the proposed method is put into practice using real data records to demonstrate its applicability in real-world scenarios. The examples given in Section 3.2.1-3.2.3 are merely illustrative of the proposed method, as artificially generated data are always constructed in some way and therefore reflect reality only to a certain extent. For the sake of brevity, only the resulting bounds and their corresponding parameters are presented for each of the three types of PSD functions, i.e. the stationary PSD function, the non-stationary non-separable EPSD function and the non-stationary separable EPSD function.

In this work, gradient-based optimisation algorithms are used to improve the efficiency and convergence of optimisation tasks. These algorithms use gradient information to iteratively adjust parameters and thus facilitate the fast determination of optimal solutions. The approach is particularly effective for smooth and continuous objective functions.

The data set used in this work is the well-known El Centro earthquake, see for instance [37]. The data set consists of two records in time domain, i.e. the record in north-south direction and the record east-west direction, which are transformed to the frequency

Table 4: Identified parameters for the Clough-Penzien PSD model fitted to the stationary El Centro data estimated with the periodogram.

		S_0	ω_f	ζ_f	ω_g	ζ_g
$\lambda = 0$	$S^{CP}\left(\omega, \underline{\boldsymbol{\theta}}^{CP}\right)$	0.0006	1.9286	0.5510	12.9481	0.6291
	$S^{CP}\left(\omega, \overline{\boldsymbol{\theta}}^{CP}\right)$	0.0016	1.0148	0.8452	12.6517	0.5864
$\lambda = 1$	$S^{CP}\left(\omega, \underline{\boldsymbol{\theta}}^{CP}\right)$	0.0004	2.0145	0.5514	11.5749	0.7840
	$S^{CP}\left(\omega, \overline{\boldsymbol{\theta}}^{CP}\right)$	0.0021	0.9164	0.8761	12.6874	0.5749
$\lambda = 2$	$S^{CP}\left(\omega, \underline{\boldsymbol{\theta}}^{CP}\right)$	0.0003	2.0461	0.5315	11.3969	0.7883
	$S^{CP}\left(\omega, \overline{\boldsymbol{\theta}}^{CP}\right)$	0.0027	0.8679	0.8912	12.7090	0.5681

domain by Eq. 3 for the stationary case and by Eq. 4 for the non-stationary case, respectively. The ensembles are depicted in Fig. 6.

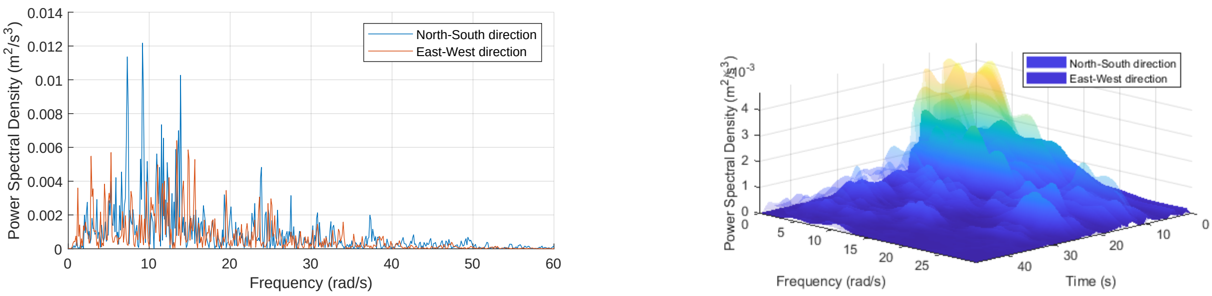

Figure 6: Ensemble of the PSDs and EPSDs of the El Centro earthquake.

The derivation of the bounds and their corresponding parameters for the estimated PSDs, i.e. for the stationary case, is described briefly in the following. The Clough-Penzien PSD model (Eq. 22) is utilised for fitting. The scaling parameter to obtain the augmented bounds is chosen to be $\lambda \in \{0, 1, 2\}$. The parameters derived by the proposed approach are given in Table 4, while the corresponding bounds are depicted in Fig. 7. The objective function values for the resulting bounds are given in Table 5.

For a more realistic representation, the non-separable EPSD function in Eq. 25 is fitted to the augmented bounds of the El Centro EPSD functions, again with scaling parameter $\lambda \in \{0, 1, 2\}$. The results for $\lambda = 0$ can be obtain in Fig. 8, while the identified bounded

Table 5: Objective function values for the resulting bounds of the stationary case.

	$S^{CP}\left(\omega, \underline{\boldsymbol{\theta}}^{CP}\right)$	$S^{CP}\left(\omega, \overline{\boldsymbol{\theta}}^{CP}\right)$
$\lambda = 0$	1.0593e-04	4.4814e-04
$\lambda = 1$	8.5038e-05	9.9150e-04
$\lambda = 2$	5.8963e-05	0.0018

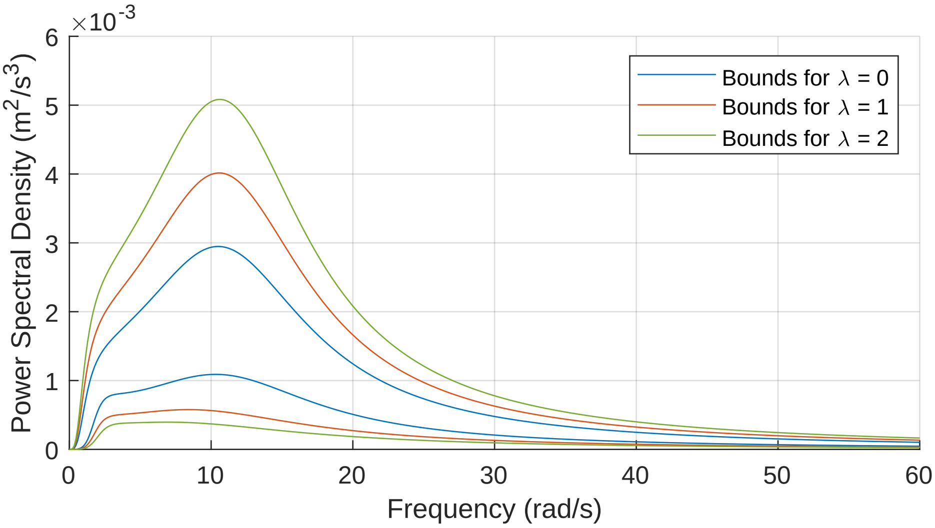

Figure 7: Comparison of the derived bounds for the El Centro data with the Clough-Penzien PSD model with $\lambda = \{0, 1, 2\}$.

Table 6: Identified parameters for the non-separable EPSD model fitted to the El Centro data.

		S_0	c	ω_g
$\lambda = 0$	$S^{non-sep}\left(\omega, t, \underline{\boldsymbol{\theta}}^{non-sep}\right)$	0.002	-0.1875	25.2118
	$S^{non-sep}\left(\omega, t, \overline{\boldsymbol{\theta}}^{non-sep}\right)$	0.0035	-0.2003	23.7434
$\lambda = 1$	$S^{non-sep}\left(\omega, t, \underline{\boldsymbol{\theta}}^{non-sep}\right)$	0.0012	-0.1826	26.6382
	$S^{non-sep}\left(\omega, t, \overline{\boldsymbol{\theta}}^{non-sep}\right)$	0.0044	-0.2007	23.4602
$\lambda = 2$	$S^{non-sep}\left(\omega, t, \underline{\boldsymbol{\theta}}^{non-sep}\right)$	0.0007	-0.1778	27.3245
	$S^{non-sep}\left(\omega, t, \overline{\boldsymbol{\theta}}^{non-sep}\right)$	0.0053	-0.201	23.2628

parameters are given in Table 6 and corresponding objective function values in Table 7.

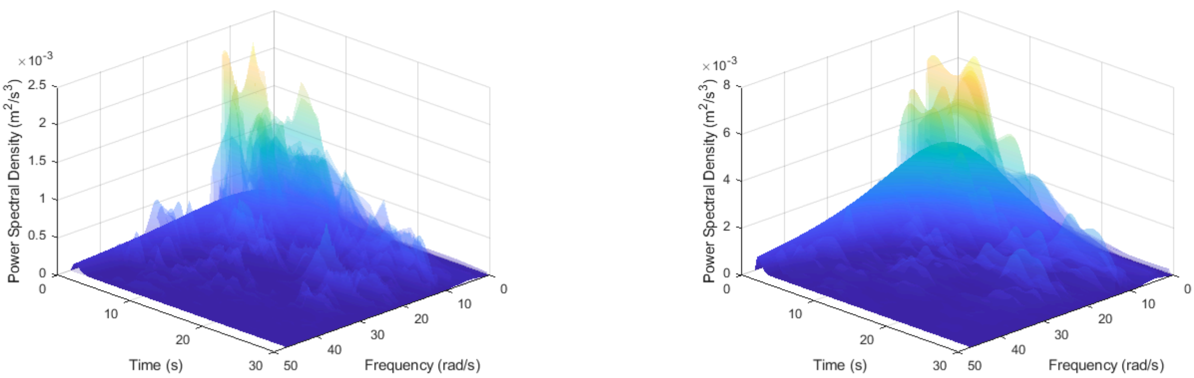

Figure 8: Comparison of augmented bounds and derived lower bound (left) and upper bound (right) for the non-separable EPSD model. The transparent representation shows the augmented bounds, the non-transparent ones are the fitted EPSDs. For both a scaling parameter of $\lambda = 0$ was utilised.

To also illustrate the flexibility of the separable EPSD, the fitting of the augmented EPSD bounds of the El Centro earthquake is illustrated for the same case, again with scaling parameter $\lambda \in \{0, 1, 2\}$. The respective bounds for $\lambda = 0$ are depicted in Fig. 9, the corresponding parameters are given in Table 8 and the objective function values are given in Table 9.

Table 7: Objective function values for the resulting bounds of the non-separable case.

	$S^{non-sep}\left(\omega, t, \underline{\boldsymbol{\theta}}^{non-sep}\right)$	$S^{non-sep}\left(\omega, t, \overline{\boldsymbol{\theta}}^{non-sep}\right)$
$\lambda = 0$	0.0536	0.1262
$\lambda = 1$	0.0354	0.2169
$\lambda = 2$	0.027	0.3388

Table 8: Identified parameters for the separable EPSD model fitted to the El Centro data.

		S_0	ω_f	ζ_f	ω_g	ζ_g	k	a	b
$\lambda = 0$	$S^{sep}\left(\omega, t, \underline{\boldsymbol{\theta}}^{sep}\right)$	1.1687	1.4511	0.7412	12.5965	0.5936	3.5507	0.1907	0.1867
	$S^{sep}\left(\omega, t, \overline{\boldsymbol{\theta}}^{sep}\right)$	1.0449	0.6871	1.7915	11.6559	0.6725	0.043	0.0403	1.4999
$\lambda = 1$	$S^{sep}\left(\omega, t, \underline{\boldsymbol{\theta}}^{sep}\right)$	1.4939	1.8465	0.4303	13.8734	0.4555	5.969	0.1903	0.1889
	$S^{sep}\left(\omega, t, \overline{\boldsymbol{\theta}}^{sep}\right)$	1.0072	0.8368	1.7974	10.9627	0.7089	0.0518	0.0403	1.5
$\lambda = 2$	$S^{sep}\left(\omega, t, \underline{\boldsymbol{\theta}}^{sep}\right)$	1.0825	1.8953	0.304	13.5149	0.3557	3.1845	0.1921	0.1898
	$S^{sep}\left(\omega, t, \overline{\boldsymbol{\theta}}^{sep}\right)$	1.0353	0.9821	1.7989	10.3706	0.7338	0.0588	0.0404	1.5

Table 9: Objective function values for the resulting bounds of the separable case.

	$S^{sep}\left(\omega, t, \underline{\boldsymbol{\theta}}^{sep}\right)$	$S^{sep}\left(\omega, t, \overline{\boldsymbol{\theta}}^{sep}\right)$
$\lambda = 0$	0.0467	0.0686
$\lambda = 1$	0.0313	0.1286
$\lambda = 2$	0.0245	0.2146

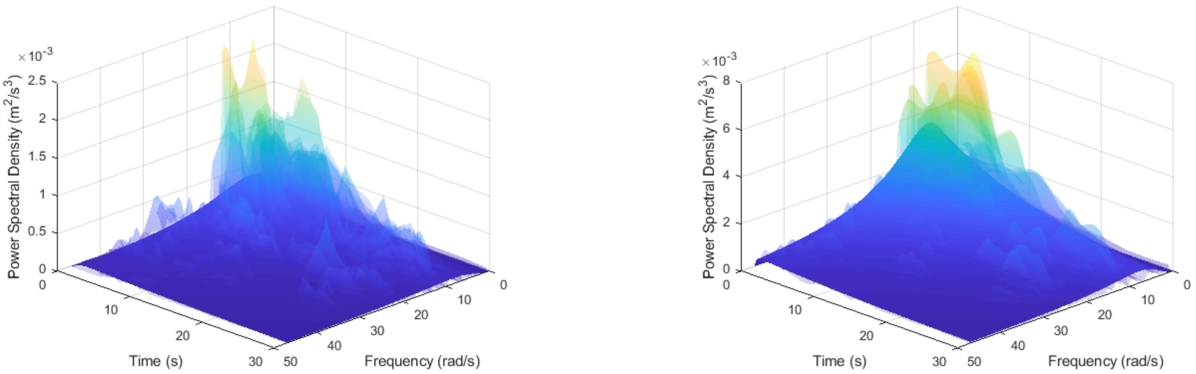

Figure 9: Comparison of augmented bounds and derived lower bound (left) and upper bound (right) for the separable EPSD model. The transparent representation shows the augmented bounds, the non-transparent ones are the fitted EPSDs. For both a scaling parameter of $\lambda = 0$ was utilised.

4.1. Comparison with imprecise power spectral density

In the pursuit of solving complex problems and achieving desired outcomes, it is often imperative to evaluate and compare different methods or approaches. This section aims into a comprehensive comparison of the proposed method with the imprecise PSD, proposed by some of the authors of this work. The imprecise PSD is an approach to bound a limited set of PSD functions in order to capture the uncertainties. The approach is described briefly in Appendix B, while the reader is referred to [20] for a detailed overview. The comparison of both methods will result in valuable insights into their respective efficiency, and suitability for specific scenarios. Through a critical analysis of their principles, implementation, and real-world performance, this examination seeks to assist decision-makers and analysts in making informed choices when choosing between these two approaches. The comparison is made for illustrative purposes and for the stationary case only, since the imprecise PSD is currently available for the stationary case only. As data set, the stationary PSDs determined from the El Centro earthquake will be utilised, see Fig. 6.

The proposed method is employed alongside the fitting of the Clough-Penzien PSD function with scaling parameter $\lambda \in \{4, 5, 6\}$. This is compared directly to the imprecise PSD, where $N_B = 8$ basis functions are utilised to derive the bounds. As it can be seen from

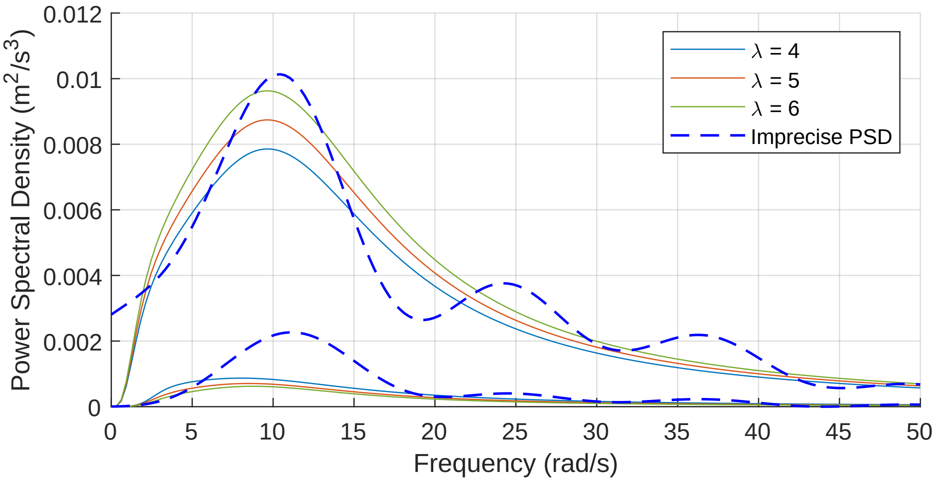

Figure 10: Comparison of the fitted Clough-Penzien spectrum with scaling parameter $\lambda \in \{4, 5, 6\}$ and the imprecise PSD with $N_B = 8$.

Table 10: Energy of the bounded PSDs derived by the Clough-Penzien PSD function and the imprecise PSD.

	Lower bound	Upper bound
$\lambda = 4$	0.0518	0.5049
$\lambda = 5$	0.0407	0.5610
$\lambda = 6$	0.0343	0.6171
Imprecise PSD	0.0879	0.5837

Fig. 10, both methods yield approximately similar results. One important difference in both methods is, that the proposed method is a model fitting approach, while the imprecise PSD is a data-driven bounding approach of a set of PSD functions. Thus, it is reasonable to choose a larger λ for a meaningful comparison, than in the previous sections. The model derived by the proposed approach is thus more conservative compared to Section 4. In addition, the proposed method delivers much smoother results, due to the fitting process, while the imprecise PSD results in more oscillating bounds, given by the fact that it is a bounding approach. However, qualitatively, similar bounds can be obtained, depending on the choice of λ. This fact is supported by the energy of the bounded PSDs, see Table 10. The energy is computed by summing up all individual PSD values for each frequency.

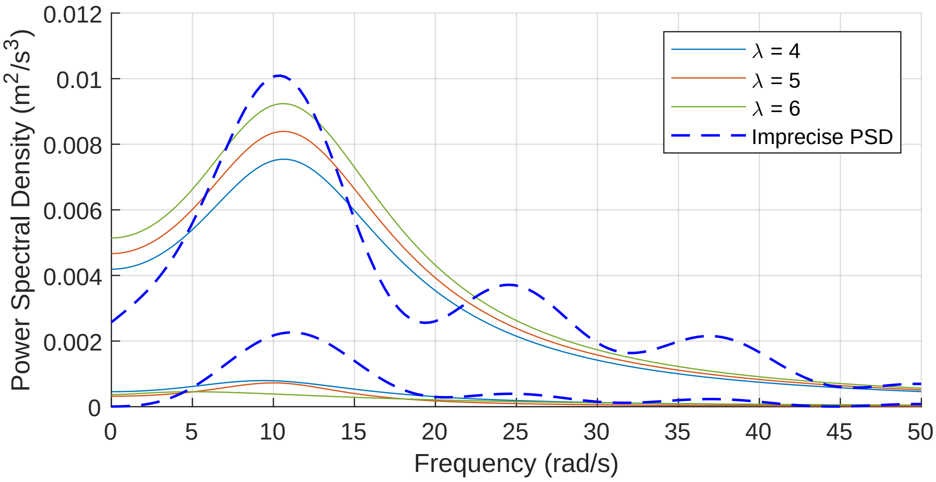

Figure 11: Comparison of the fitted Kanai-Tajimi spectrum with scaling parameter $\lambda \in \{4, 5, 6\}$ and the imprecise PSD with $N_B = 8$.

Table 11: Energy of the bounded PSDs derived by the Kanai-Tajimi PSD function and the imprecise PSD.

	Lower bound	Upper bound
$\lambda = 4$	0.0499	0.5013
$\lambda = 5$	0.0365	0.5572
$\lambda = 6$	0.0336	0.6131
Imprecise PSD	0.0879	0.5837

In a second comparison, the Kanai-Tajimi PSD function (Eq. 21) will be utilised to derived the bounds of the El Centro PSD estimates with the proposed method. The bounds are derived by using a scaling parameter of $\lambda \in \{4, 5, 6\}$. Again, the imprecise PSD bounds with $N_B = 8$ are utilised for a comparison. As it can be obtained from Fig. 11, the bounds of the Kanai-Tajimi PSD fit are very smooth, naturally for an analytical model. However, small but neglectable differences can be obtained, mostly due to the oscillating nature of the imprecise PSD. In general, a reasonably accurate approximation can be achieved, which is supported by the determined energy in Table 11.

5. Conclusions

This study has introduced a robust methodology for the determination of interval parameters within physically derived stationary and evolutionary PSDs models. The resulting bounded parameters offer a pivotal foundation for the assessment of upper and lower failure probabilities as an integral part of structural reliability evaluations. Importantly, this approach is not limited to the PSD/EPSD models utilised in this work. It can be used with a wide range of models, making it flexible for different cases. Although this method is fast and efficient at optimising parameter bounds, a significant challenge is choosing the right model to match the data accurately. Since optimising the bounds is fast, it is worth considering using multiple models and picking the best-fitting one. In this work, primarily gradient-based optimisation algorithms have been utilised, which yielded in satisfactory results. However, it is essential to acknowledge that optimisation problems of this nature often entail numerous local minima. Although no issues has been identified in this work, exploring alternative classes of optimisation methods, such as particle swarm optimisation, may prove advantageous, particularly when dealing with real-world data. Furthermore, the selection of an appropriately scaling parameter is of paramount importance. An excessively large scaling parameter can, depending on the specific characteristics of the system under investigation, lead to a bounded failure probability of $p_f = [0, 1]$. While this outcome is theoretically correct, it lacks meaningful information and falls short of aligning with the intended objectives of the proposed approach. Hence, the reasonable choice of the scaling parameter remains a pivotal consideration in the methodology, which ensures the practicality and relevance of the resulting failure probability assessments. An open issue is the efficient propagation of derived bounds through a system under investigation. Classical double-loop approaches may yield good results, however, for this class of problems advantageous solutions may be required. Future developments will focus on such an efficient propagation method of the bounds to obtain a bounded failure probability.

CRediT author statement

Marco Behrendt: Methodology, Formal analysis, Visualization, Validation, Software, Writing - Original Draft. **Chao Dang:** Conceptualization, Methodology, Validation, Writing - Review & Editing. **Michael Beer:** Project administration, Supervision, Conceptualization, Funding acquisition, Writing - Review & Editing.

Acknowledgement

Chao Dang would like to thank the support of the China Scholarship Council (CSC).

Appendix A. Time-modulating functions

There are several time-modulating functions available in the literature, which may fit better to the problem at hand. See for instance [38, 39]. In contrast to the continuous time-modulating function given in Eq. 29, these envelope functions are piecewise-defined:

$$g_2(t) = \begin{cases} \left(0.8 + 0.2\frac{t}{t_a}\right) & \text{for } t < t_a \\ 1 & \text{for } t_a \leq t \leq t_b \\ \left(\frac{t_b}{t}\right)^{\frac{2}{3}} & \text{for } t > t_b \end{cases} \tag{A.1}$$

$$g_3(t) = \begin{cases} \left(\frac{t}{t_a}\right)^2 & \text{for } t < t_a \\ 1 & \text{for } t_a \leq t < t_b \\ \exp\left(-\alpha(t - t_b)\right) & \text{for } t \geq t_b \end{cases} \tag{A.2}$$

Appendix B. Imprecise power spectral density function

The imprecise PSD function will be described in the following briefly. For a detailed overview refer to [20].

A set of radial basis functions

$$\phi_i(x) = e^{-\left(||x-c_i||\cdot b_{\phi_i}\right)^2} \tag{B.1}$$

constitute a radial basis function network

$$y(x) = \sum_{i=1}^{N_B} w_i \; \phi_i(||x - c_i|| \cdot b_{\phi_i}) + b_0 \qquad x \in \mathbb{R}^{N_\omega}. \tag{B.2}$$

Such a network will be used to determine the bounded PSD model, the imprecise PSD. Therefore, the so-called basis power spectrum S_{basis} is computed, which can be, for instance the midpoint spectrum

$$S_{basis}(\omega_n) = \frac{1}{2}\left(S_{max}(\omega_n) + S_{min}(\omega_n)\right). \tag{B.3}$$

With the resulting basis power spectrum a first approximation of the ensemble of PSD functions is derived, while the weights and bias can be obtained. To identify an upper and lower bound, the expression in Eq. B.2 will be reformulated

$$\begin{aligned} \underline{S_{opt}}(\omega_n; w^{low}) &= \sum_{i=1}^{N_B} w_i^{low} \phi_i + b_0, \\ \overline{S_{opt}}(\omega_n; w^{up}) &= \sum_{i=1}^{N_B} w_i^{up} \phi_i + b_0, \end{aligned} \tag{B.4}$$

to modify the weights as part of an optimisation

$$\begin{aligned} \min \quad & \left|\left|\overline{S_{opt}}(\omega_n; w^{up}) - \underline{S_{opt}}(\omega_n; w^{low})\right|\right| \\ \text{s.t.} \quad & \overline{S_{opt}}(\omega_n; w^{up}) \geq S_{max}(\omega_n) \\ & \underline{S_{opt}}(\omega_n; w^{low}) \leq S_{min}(\omega_n) \\ & \underline{S_{opt}}(\omega_n; w^{low}) \geq 0 \\ & w^{low} \leq w^{up}. \end{aligned} \tag{B.5}$$

Thus, an upper bound $\overline{S_{opt}}$ and lower bound $\underline{S_{opt}}$ can be obtained.

References

[1] Y.-K. Lin, G.-Q. Cai, Probabilistic Structural Dynamics: Advanced Theory and Applications, McGraw-Hill New York, 1995.

[2] A. K. Chopra, Dynamics of Structures: Theory and Applications to Earthquake Engineering, Prentice-Hall, 1995.

[3] J. Li, J. Chen, Stochastic Dynamics of Structures, John Wiley & Sons, 2009.

[4] M. Grigoriu, Stochastic Calculus: Applications in Science and Engineering, Springer, 2002. doi:https://doi.org/10.1007/978-0-8176-8228-6.

[5] L. D. Lutes, S. Sarkani, Random Vibrations: Analysis of Structural and Mechanical Systems, Butterworth-Heinemann, 2004.

[6] C. Wang, Structural Reliability and Time-Dependent Reliability, Springer Series in Reliability Engineering, Springer International Publishing, Cham, 2021. URL: http://link.springer.com/10.1007/978-3-030-62505-4. doi:10.1007/978-3-030-62505-4.

[7] D. E. Newland, An Introduction to Random Vibrations, Spectral & Wavelet Analysis, Courier Corporation, 2012.

[8] R. A. Muller, G. J. MacDonald, Ice ages and astronomical causes: data, spectral analysis and mechanisms, Springer Science & Business Media, 2002.

[9] M. B. Priestley, Evolutionary spectra and non-stationary processes, Journal of the Royal Statistical Society. Series B (Methodological) 27 (1965) 204–237.

[10] M. Priestley, Power spectral analysis of non-stationary random processes, Journal of Sound and Vibration 6 (1967) 86–97. doi:https://doi.org/10.1016/0022-460X(67)90160-5.

[11] M. Priestley, Spectral Analysis and Time Series, Probability and mathematical statistics : A series of monographs and textbooks, Academic Press, 1982.

[12] E. Nikolaidis, D. M. Ghiocel, S. Singhal, Engineering Design Reliability Handbook, 1 ed., CRC press, 2004. doi:https://doi.org/10.1201/9780203483930.

[13] M. Grigoriu, Stochastic systems: Uncertainty Quantification and Propagation, Springer Science & Business Media, 2012. doi:https://doi.org/10.1007/978-1-4471-2327-9.

[14] M. G. R. Faes, D. Moens, Recent trends in the modeling and quantification of non-probabilistic uncertainty, Archives of Computational Methods in Engineering 27 (2020) 633–671. URL: https://link.springer.com/article/10.1007/s11831-019-09327-x. doi:https://doi.org/10.1007/s11831-019-09327-x.

[15] M. Beer, S. Ferson, V. Kreinovich, Imprecise probabilities in engineering analyses, Mechanical Systems and Signal Processing 37 (2013) 4 – 29. doi:10.1016/j.ymssp.2013.01.024.

[16] R. Rocchetta, Q. Gao, M. Petkovic, Soft-constrained interval predictor models and epistemic reliability intervals: A new tool for uncertainty quantification with limited experimental data, Mechanical Systems and Signal Processing 161 (2021) 107973. URL: https://www.sciencedirect.com/science/article/pii/S088832702100368X. doi:https://doi.org/10.1016/j.ymssp.2021.107973.

[17] A. Gray, A. Wimbush, M. de Angelis, P. Hristov, D. Calleja, E. Miralles-Dolz, R. Rocchetta, From inference to design: A comprehensive framework for uncertainty quantification in engineering with

limited information, Mechanical Systems and Signal Processing 165 (2022) 108210. URL: https://www.sciencedirect.com/science/article/pii/S0888327021005859. doi:https://doi.org/10.1016/j.ymssp.2021.108210.

[18] M. G. R. Faes, M. A. Valdebenito, D. Moens, M. Beer, Bounding the first excursion probability of linear structures subjected to imprecise stochastic loading, Computers & Structures 239 (2020) 106320. URL: https://www.sciencedirect.com/science/article/pii/S0045794920301231. doi:https://doi.org/10.1016/j.compstruc.2020.106320.

[19] G. Muscolino, F. Genovese, A. Sofi, Reliability Bounds for Structural Systems Subjected to a Set of Recorded Accelerograms Leading to Imprecise Seismic Power Spectrum, ASCE-ASME Journal of Risk and Uncertainty in Engineering Systems, Part A: Civil Engineering 8 (2022) 04022009. doi:10.1061/AJRUA6.0001215.

[20] M. Behrendt, M. G. R. Faes, M. A. Valdebenito, M. Beer, Estimation of an imprecise power spectral density function with optimised bounds from scarce data for epistemic uncertainty quantification, Mechanical Systems and Signal Processing 189 (2023) 110072. URL: https://www.sciencedirect.com/science/article/pii/S0888327022011402. doi:https://doi.org/10.1016/j.ymssp.2022.110072.

[21] K. Kanai, Semi-empirical formula for the seismic characteristics of the ground, Bulletin of the Earthquake Research Institute 35 (1957) 309–325.

[22] H. Tajimi, A statistical method of determining the maximum response of a building structure during an earthquake, in: Proceedings of the 2nd world conference of earthquake engineering, volume 11, 1960, pp. 781–797.

[23] R. W. Clough, J. Penzien, Dynamics of structures, McGraw-Hill, 1975.

[24] M. S. Bartlett, Smoothing periodograms from time-series with continuous spectra, Nature 161 (1948) 686–687.

[25] M. S. Bartlett, Periodogram analysis and continuous spectra, Biometrika 37 (1950) 1–16. URL: https://doi.org/10.1093/biomet/37.1-2.1. doi:10.1093/biomet/37.1-2.1. arXiv:https://academic.oup.com/biomet/article-pdf/37/1-2/1/486591/37-1-2-1.pdf.

[26] P. Welch, The use of fast Fourier transform for the estimation of power spectra: A method based on time averaging over short, modified periodograms, IEEE Transactions on Audio and Electroacoustics 15 (1967) 70–73. doi:10.1109/TAU.1967.1161901.

[27] P. D. Spanos, G. Failla, Evolutionary spectra estimation using wavelets, Journal of Engineering Mechanics 130 (2004) 952–960. doi:10.1061/(ASCE)0733-9399(2004)130:8(952).

[28] D. E. Newland, Ridge and Phase Identification in the Frequency Analysis of Transient Signals by Harmonic Wavelets, Journal of Vibration and Acoustics 121 (1999) 149–155. URL: https://doi.org/10.1115/1.2893957. doi:10.1115/1.2893957.

[29] Z. Huang, Y.-L. Xu, T. Tao, Multi-taper S-transform method for evolutionary spectrum estimation, Mechanical Systems and Signal Processing 168 (2022) 108667. URL: https://www.sciencedirect.com/science/article/pii/S0888327021009912. doi:https://doi.org/10.1016/j.ymssp.2021.108667.

[30] Z. Huang, Y.-L. Xu, A Multi-Taper S-Transform Method for Spectral Estimation of Stationary Processes, IEEE Transactions on Signal Processing 69 (2021) 1452–1467. doi:10.1109/TSP.2021.3057488.

[31] M. Shinozuka, G. Deodatis, Simulation of stochastic processes by spectral representation, Applied Mechanics Reviews 44 (1991) 191–204. doi:10.1115/1.3119501.

[32] J. Liang, S. R. Chaudhuri, M. Shinozuka, Simulation of nonstationary stochastic processes by spectral representation, Journal of Engineering Mechanics 133 (2007) 616–627.

[33] R. J. Tibshirani, B. Efron, An introduction to the bootstrap, Monographs on statistics and applied probability 57 (1993).

[34] A. Zerva, Spatial Variation of Seismic Ground Motions: Modeling and Engineering Applications, CRC Press, 2009.

[35] G. Deodatis, Non-stationary stochastic vector processes: seismic ground motion applications, Probabilistic Engineering Mechanics 11 (1996) 149–167. URL: https://www.sciencedirect.com/science/article/pii/0266892096000070. doi:https://doi.org/10.1016/0266-8920(96)00007-0.

[36] P. Spanos, I. Kougioumtzoglou, Harmonic wavelets based statistical linearization for response evolutionary power spectrum determination, Probabilistic Engineering Mechanics 27 (2012) 57 – 68. URL: http://www.sciencedirect.com/science/article/pii/S0266892011000294. doi:https://doi.org/10.1016/j.probengmech.2011.05.008, the IUTAM Symposium on Nonlinear Stochastic Dynamics and Control.

[37] C. A. Goulet, T. Kishida, T. D. Ancheta, C. H. Cramer, R. B. Darragh, W. J. Silva, Y. M. Hashash, J. Harmon, G. A. Parker, J. P. Stewart, R. R. Youngs, PEER NGA-East database, Earthquake Spectra 37 (2021) 1331–1353. URL: https://doi.org/10.1177/87552930211015695. doi:10.1177/87552930211015695. arXiv:https://doi.org/10.1177/87552930211015695.

[38] P. D. Spanos, J. Tezcan, P. Tratskas, Stochastic processes evolutionary spectrum estimation via harmonic wavelets, Computer Methods in Applied Mechanics and Engineering 194 (2005) 1367–1383. URL: https://www.sciencedirect.com/science/article/pii/S0045782504003974. doi:https://doi.org/10.1016/j.cma.2004.06.039, special Issue on Computational Methods in Stochastic Mechanics and Reliability Analysis.

[39] M. Shields, G. Deodatis, Estimation of evolutionary spectra for simulation of non-stationary and non-gaussian stochastic processes, Computers & Structures 126 (2013) 149–163. URL: https://www.sciencedirect.com/science/article/pii/S0045794913000552. doi:https://doi.org/10.1016/j.compstruc.2013.02.007, Uncertainty Quantification in structural analysis and design: To commemo-

rate Professor Gerhart I. Schueller for his life-time contribution in the area of computational stochastic mechanics.